A. Reshetnikov [1], M. Jaya [2], S. Buske [3], J. Kummerow [1], and S.A. Shapiro [1]
[1] Freie Universität Berlin, Germany
[2] GFZ Potsdam, Germany
[3] TU Bergakademie Freiberg, Germany
anton@geophysik.fu-berlin.de

Characterisation of a geothermal reservoir using microseismic data

Freie Universität Berlin

Summary

In this work we considered the geological structure at the German deep drill site (KTB) as a prototype of a geothermal system. We used microseismic data in combination with surface seismic imaging results for characterization of the geothermal reservoir. First, we located microseismicity induced by fluid injection experiment. Then, we applied SBRC approach and estimated rock diffusivity using three clouds of microseismicity which corresponded to two different fault zones and background rock. Using the large scale surface reflection imaging result and assuming positive correlation between the seismic reflectivity and the hydraulic permeability, we constructed 3D permeability model. Finally, we applied our reflection microseismic imaging approach to the microseismic waveforms recorded at single three-component geophone and constructed the high-resolution image of inner structure of the fault zone.

KTB project

The German Deep Drilling Site (KTB) is located on basement rock at the western margin of the Bohemian Massif. About 4 km west of the KTB, the Franconian Lineament outcrops, a NW-SE trending, deep-reaching system of thrust faults, which separates the basement block from Permo-Mesozoic sediments.

During a one-year hydraulic experiment in 2004/2005, water was constantly injected in the open-bottom section of the KTB pilot hole at 4 km depth, where the borehole intersects one of these faults. This fault (SE2 reflector) is characterised by steeply dipping seismic reflections (Harjes et al. (1997)).

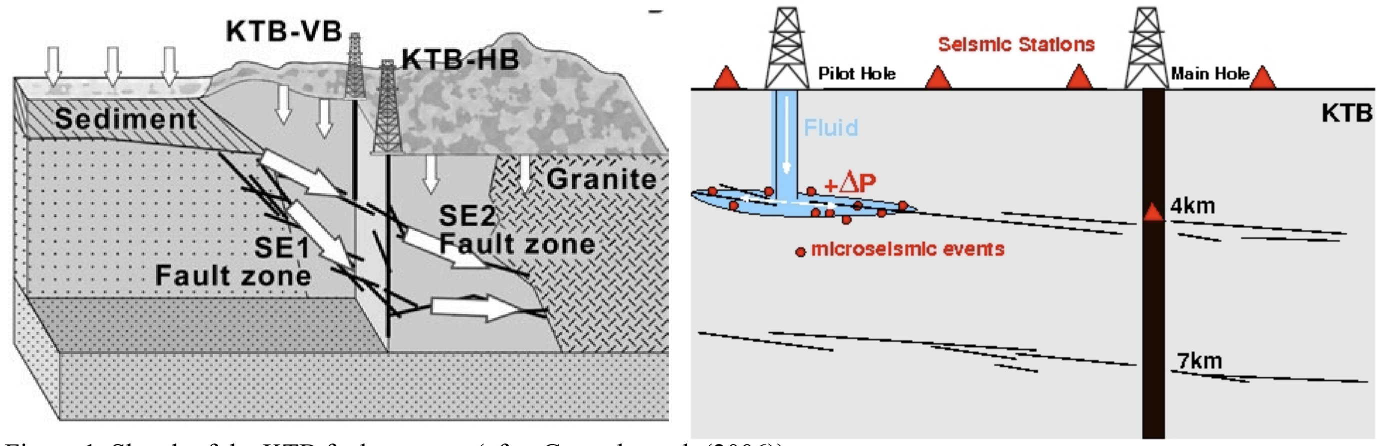

Figure 1. Sketch of the KTB fault systems (after Graessle et al. (2006)).

The seismicity was monitored by a seismic network, which consisted of a borehole seismometer in KTB main hole at 200 m horizontal distance from the injection source and variable number of near-surface stations (on average 10–15 stations). Most of the stations were installed within radius of 3 km from the KTB. All instruments were 3-component seismometers and data were recorded continuously at sample rates 200–1000 Hz.

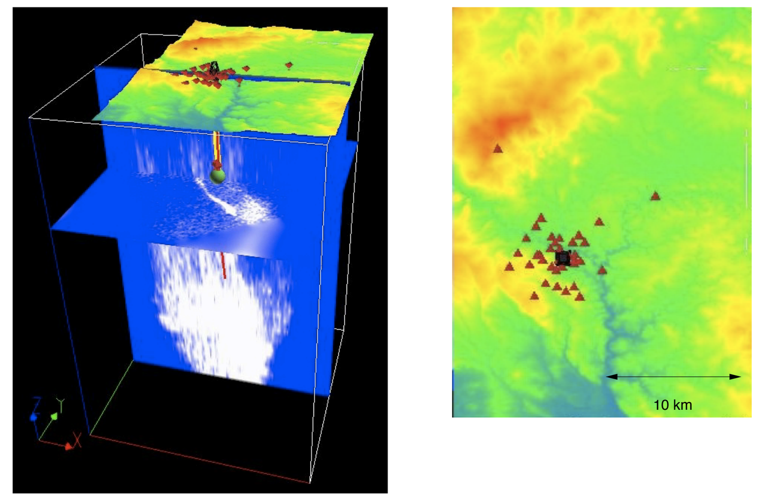

Figure 2. Left: Configuration of the KTB injection test in 4 km depth (green bullet) and the seismic sensors (red diamonds). Also shown is the seismic reflectivity after Busker (1999). Right: Map view of the station distribution; black square is the KTB site.

Microseismicity location

The cumulative number of events detected by near-surface stations was 146, and more than 3000 for the borehole sensor. All events were small with magnitudes in the range of -3.0 to +0.3. Only the events which were also recorded by near-surface stations could be precisely located. We applied a two- step location procedure: absolute location was first determined by a grid-search algorithm (NonLinLoc, Lomax et al. (2000)) in a local 3D velocity model. These locations were then refined by a double-difference relocation (Waldhauser and Ellsworth (2000), Waldhauser (2001)).

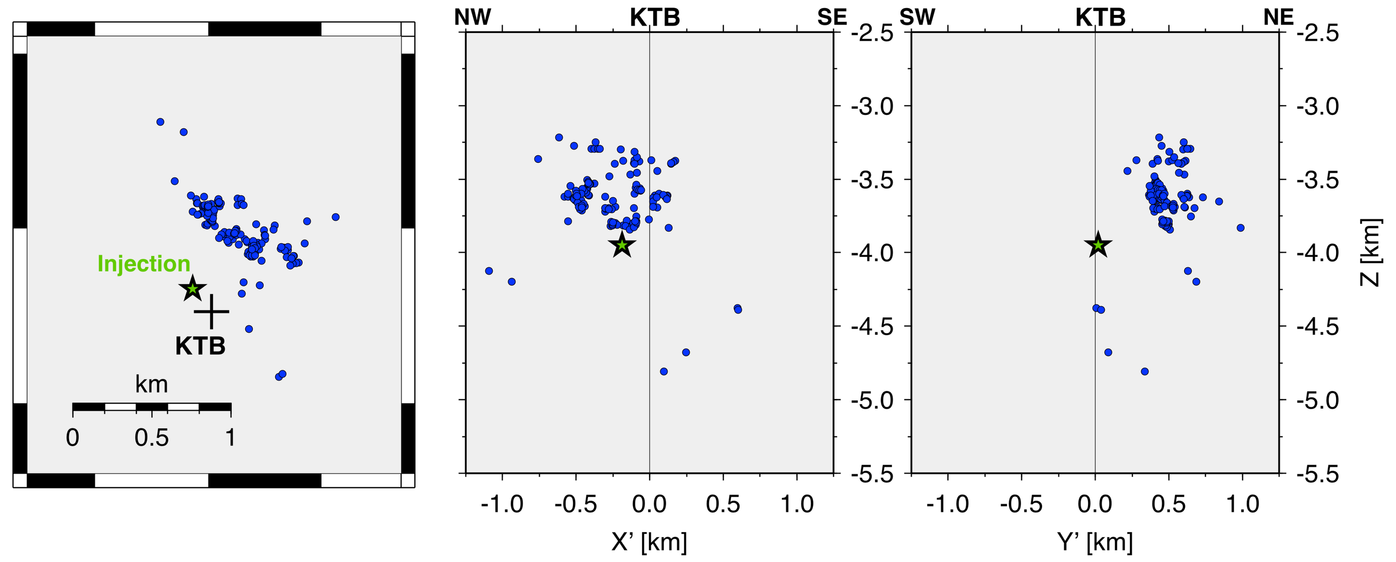

Figure 3. Location of induced microevents in plan view (left) and two side views (vertical NW-SE and SW-NE planes, middle and right).

Surface seismic imaging and seismic attributes analysis

In order to get a large scale model of the fault zones we used the image obtained from a 3-D pre-stack depth migration of the ISO89-3D data set (Buske (1999)). To enhance specific geological features which were we not able to obtain using only the original migrated seismic data we also conducted additional seismic attributes analysis. The seismic attributes were represented in the form of absolute energy values calculated by Hilbert transform of migrated seismic data (Jaya et al. (2009)).

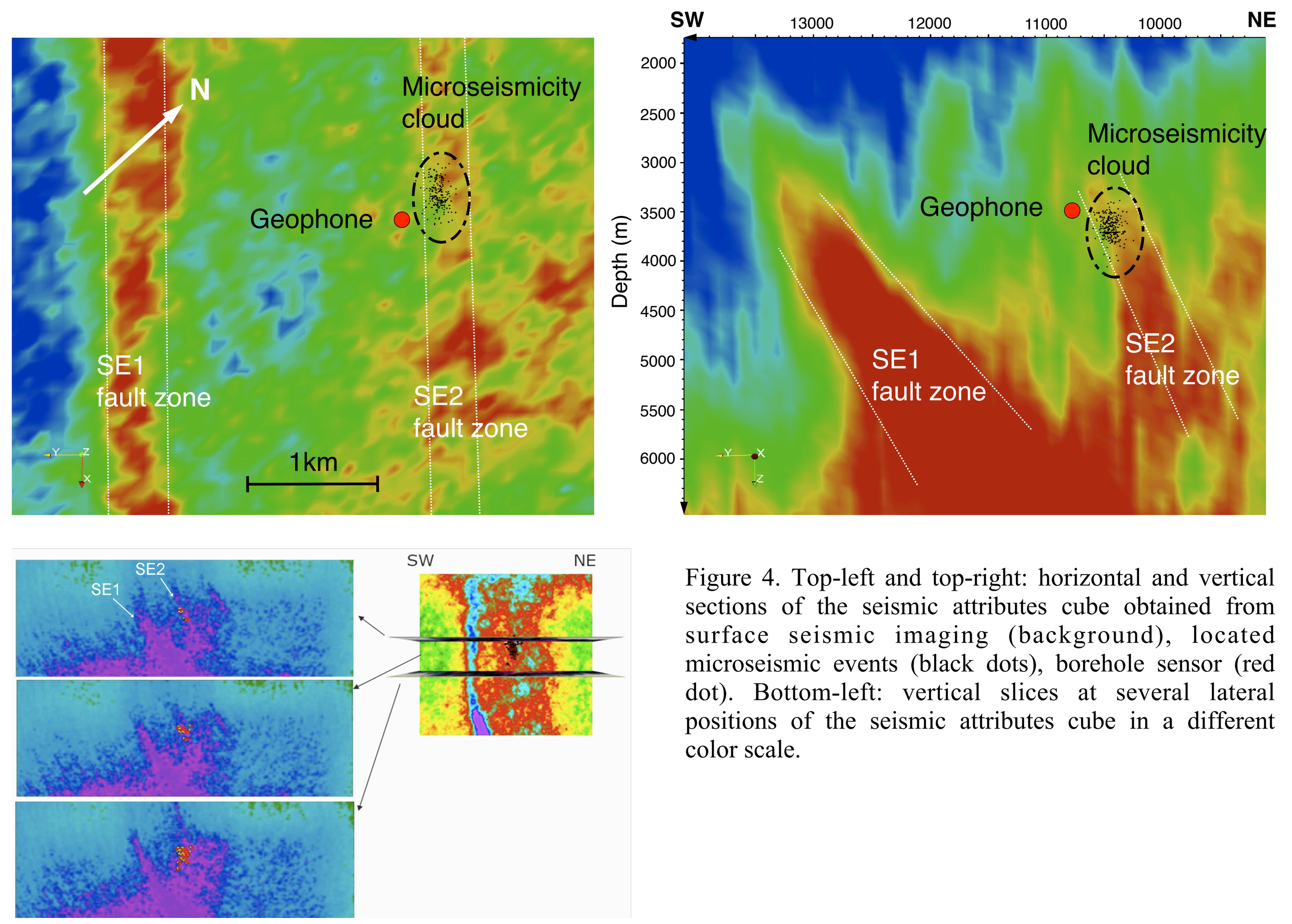

Figure 4. Top-left and top-right: horizontal and vertical sections of the seismic attributes cube obtained from surface seismic imaging (background), located microseismic events (black dots), borehole sensor (red dot). Bottom-left: vertical slices at several lateral positions of the seismic attributes cube in a different color scale.

Construction of permeability model

Shapiro et al. (2006) applied Seismicity Based Reservoir Characterization (SBRC) approach to the three stages of the fluid injection experiment and estimated rock diffusivity using three clouds of microseismicity at 9 km depth which corresponded to SE1 fault zone, at 4 km depth (SE2 reflector) and 5.4 km depth (background rocks).

D_{SE1}: **0.05 m²/s – 0.2 m²/s**

D_{SE2}: **0.01 m²/s – 0.02 m²/s**

$D_{Background}$: **0.004 m²/s – 0.01 m²/s**

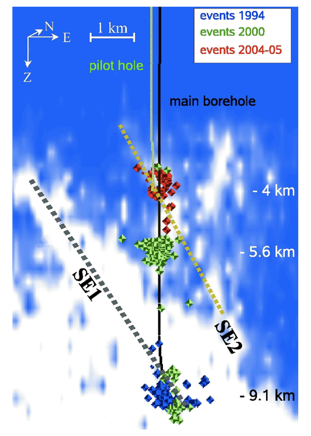

Figure 5. Seismicity induced by injection experiments of years 1994 (blue), 2000 (green) and 2004/2005 (red). Depth migrated image ISO89-3D is shown on the background.

Refinement of the background diffusivity

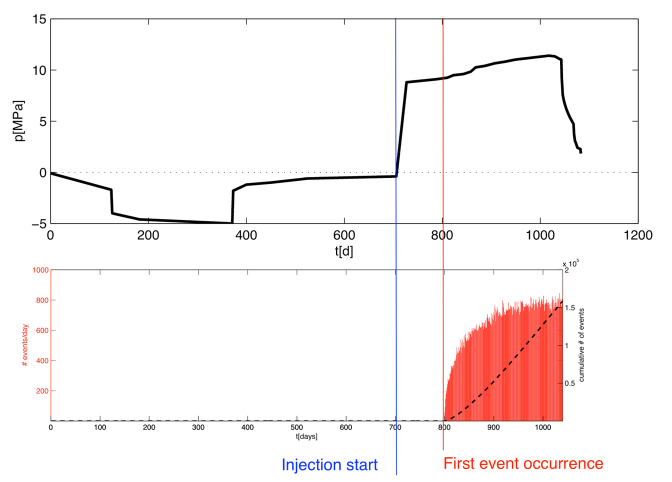

Figure 6. Top: injection pressure. Bottom: seismicity rate and cumulative number of events.

The time delay between injection start and first event occurrence is mainly controlled by background diffusivity ⇒ background diffusivity can be specified by fitting this delay (C. Langenbruch pers. coop.).

$$\frac{\partial P}{\partial t} = D\nabla^2 p$$

$D_{BG} \approx$ **0.002 m²/s**

Permeability tensor estimation

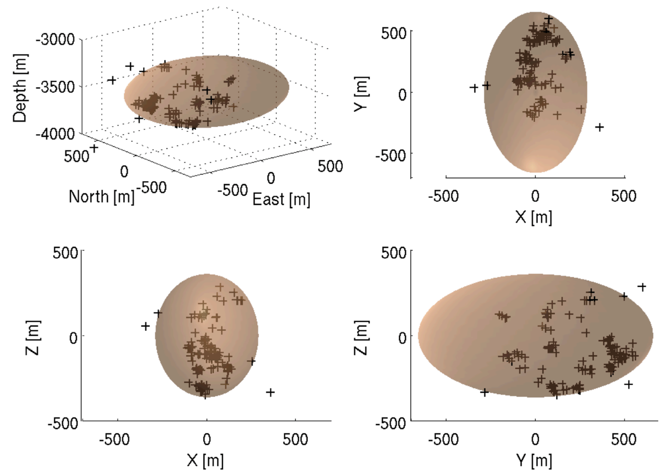

Figure 7. Ellipsoidal envelope of the microseismic cloud representing permeability tensor.

Estimated half-radiuses:
a = 650 m, b = 290 m, c = 360 m

$a^2:b^2:c^2$ relation can be used as the principal components of the permeability tensor (C. Dinske pers. coop.)

$$K_{Tensorial} = \begin{pmatrix} 1.99 & 0 & 0 \\ 0 & 0.40 & 0 \\ 0 & 0 & 0.61 \end{pmatrix} K_{Scalar}$$

In order to construct 3D permeability model we made an assumption about the positive correlation between the seismic reflectivity and the hydraulic diffusivity. Our suggested permeability model consists of three bodies: isotropic body of background permeability, low permeable SE2 fault zone and high permeable SE1 zone. Using seismic attributes as a reference map of the reflectivity, we separated the whole volume into three parts by specifying two thresholds for the attribute values.

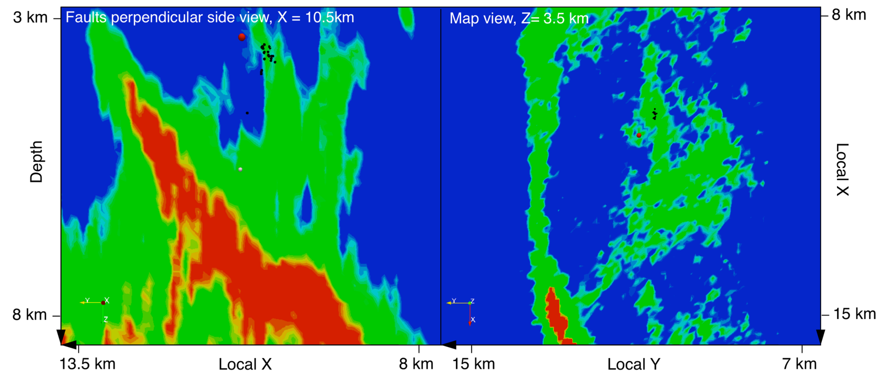

D = K ∗ N/η

N ≈ **1.68 ∗ 10^{11} Pa** – poroelastic modulus

η = **1.9 ∗ 10^{4} Pa s** – viscosity of the fluid (Rothert, 2004)

$K_{SE1} \approx$ **1.1 ∗ 10^{-16} m² = 1.1 ∗ 10^{-4} D**

$K_{SE2} \approx$ **1.6 ∗ 10^{-17} m² = 1.6 ∗ 10^{-5} D**

$K_{BG} \approx$ **2.2 ∗ 10^{-18} m² = 2.2 ∗ 10^{-6} D**

Figure 8. Obtained permeability model. Left: vertical section. Right: horizontal section.

Microseismic reflection imaging

In order to get a high resolution image of SE2 fault zone we applied our microseismic imaging approach (Reshetnikov et al. (2010)) to the waveforms recorded at the borehole sensor. Using Fresnel-Volume-Migration (Buske et. al. (2009)) technique we constructed 3D images of the data between P- and S- first arrivals which we interpreted as PP reflections. There was a complicated network of reflectors revealed in the vicinity of microseismicity cloud which belonged to SE2 reflector. Obtained result is mainly consistent with seismic attributes by the location and dip. Furthermore, it provides a more detailed image of the fine structure of the fault zone due to higher frequencies used in our study (60 – 350 Hz).

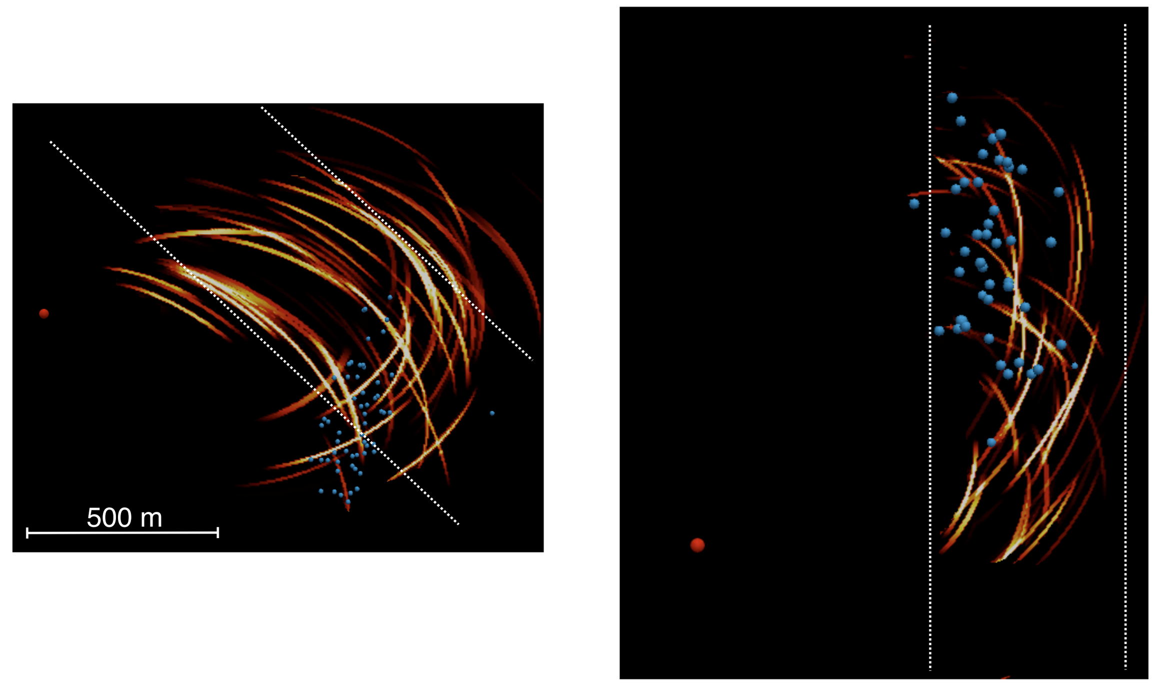

Figure 10. Image of the PP reflected waves from 414 microseismic events (blue dots) recorded at single 3C geophone (red dot). Left: vertical section. Right: horizontal section.

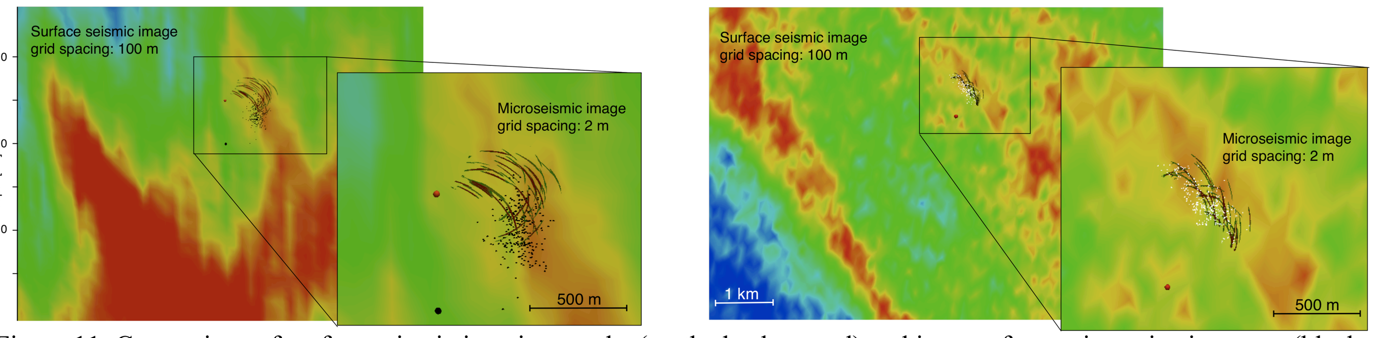

Figure 11. Comparison of surface seismic imaging results (on the background) and images from microseismic events (black slices). Red point — geophone position, black dots — microseismic events. Left: vertical section. Right: horizontal section.

Acknowledgements

The authors are indebted to appreciate the support of the German Ministry for Research and Education for the project "MeProRisk: Novel Methods for Prediction and Risk Assessment in Exploration, Development and Utilisation of Geothermal Reservoir" (Project-ID: 03SF0326B).

References

Buske, S. (1999). 3-d prestack Kirchhoff migration of the ISO89-3D data set. Pure Appl. Geophys., 156:157–171.

Buske, S., Gutjahr, S., and Sick, C. (2009). Fresnel volume migration of single-component seismic data. Geophysics, 74:WCA47-WCA55, doi:10.1190/1.3223187.

Graesle, W., Kessels, W., Kumpel, H.-J. and X. Li (2006). Hydraulic observations from a one year fluid production test in the 4000 m deep KTB pilot borehole. Geofluids, 6, 8–23.

Harjes, H.-P., Bram, K., Dürbaum, H.-J., Gebrande, H., Hirschmann, G., Janik, M., Klöckner, M., Lüschen, E., Rabbel, W., Simon, M., Thomas, R., Tormann, J., and Wenzel, F. (1997). Origin and nature of crustal reflections: Results from integrated seismic measurements at the KTB superdeep drilling site. J. Geophys. Res., 102:18267–18288.

Jaya, M. S., Buske, S., Kummerow, J., Reshetnikov, A. and Shapiro, S. A. (2009). Seismic attribute analysis of the 3-d depth-migrated image and its correlation with the induced microseismicity. Expanded abstracts, EAGE 71st annual meeting and technical exhibition, Amsterdam.

Kummerow, J., Shapiro, S., Asch, G., Dinske, C. and Rothert, E. (2006). Interpretation of fluid-induced microseismicity at 4km depth at the German Deep Drilling Site (KTB). Expanded abstracts, D013., EAGE 68th annual meeting and technical exhibition, Vienna.

Lomax, A., Virieux, J., Volant, P., and Berge, C. (2000). Probabilistic earthquake location in 3D and layered models: Introduction of a Metropolis-Gibbs method and comparison with linear locations. In Advances in Seismic Event Location. Thurber and Rabinowitz (eds.), pages 101–134.

Reshetnikov, A., Buske, S., and Shapiro, S. A. (2010). Seismic imaging using microseismic events: Results from the San Andreas Fault system at SAFOD. J. Geophys. Res., 115:B12324.

Rothert, E. (2004). Fluid induced microseismicity: Data modeling and inversion for hydraulic properties of rocks. PhD thesis.

Waldhauser, F. (2001). Hypodd: A computer program to compute double-difference hypocenter locations. Report, U.S. Geol. Surv. Open File Rep., 01-113.

Waldhauser, F. and Ellsworth, W. (2000). A double-difference earthquake location algorithm: Method and application to the northern Hayward fault, California. Bull. Seism. Soc. Am., 90:1353–1368.